

Statics and Dynamics of Incommensurate Spin Order in a Geometrically Frustrated Antiferromagnet CdCr_2O_4

J.-H. Chung,¹ M. Matsuda,² S.-H. Lee,³ K. Kakurai,² H. Ueda,⁴ T.J. Sato,⁴ H. Takagi,⁵ K.-P. Hong,⁶ and S. Park⁶

¹*NIST Center for Neutron Research, National Institute of Standards and Technology, Gaithersburg, Maryland 20899-8552, USA*

²*Advanced Science Research Center, Japan Atomic Energy Research Institute, Tokai, Ibaraki 319-1195, Japan*

³*Department of Physics, University of Virginia, Charlottesville, Virginia 22904, USA*

⁴*Institute for Solid State Physics, University of Tokyo, Kashiwa, Chiba 277-8581, Japan*

⁵*Graduate School of Frontier Science, University of Tokyo, Kashiwa, Chiba 277-8581, Japan*

⁶*HANARO Center, Korea Atomic Energy Research Institute, Daejeon, Korea*

(Received 21 April 2005; published 8 December 2005)

Using elastic and inelastic neutron scattering we show that a cubic spinel, CdCr_2O_4 , undergoes an elongation along the c axis ($c > a = b$) at its spin-Peierls-like phase transition at $T_N = 7.8$ K. The Néel phase ($T < T_N$) has an incommensurate spin structure with a characteristic wave vector $\mathbf{Q}_M = (0, \delta, 1)$ with $\delta \sim 0.09$ and with spins lying on the ac plane. This is in stark contrast to another well-known Cr-based spinel, ZnCr_2O_4 , that undergoes a c -axis contraction and a commensurate spin order. The magnetic excitation of the incommensurate Néel state has a weak anisotropy gap of 0.6 meV and it consists of at least three bands extending up to 5 meV.

DOI: 10.1103/PhysRevLett.95.247204

PACS numbers: 75.40.Gb, 75.25.+z, 75.30.Ds, 75.50.Ee

When a transition metal oxide has degeneracy, orbital or magnetic, a novel phase transition can occur through the coupling of the relevant degrees of freedom to the lattice to lift the degeneracy. A well-known example is the Jahn-Teller lattice distortion that involves either doubly degenerate e_g orbitals or triply degenerate t_{2g} orbitals [1,2]. Geometrically frustrated magnets provide a fertile ground for similar novel phase transitions because the degeneracy can be macroscopic both for quantum and for classical spins [3]. Until now the most frustrating system known is the one that consists of a network of corner-sharing tetrahedra, the pyrochlore lattice, with the simplest spin Hamiltonian; $\mathcal{H}_1 = -J \sum_{NN} \mathbf{S}_i \cdot \mathbf{S}_j$ with isotropic antiferromagnetic nearest neighbor interactions only. Theoretically, it has been shown that in the ideal case, the spins alone cannot order even at zero temperature [4,5]. Experimentally the magnetic lattice can be realized in several materials such as in the pyrochlores $\text{A}_2\text{B}_2\text{O}_7$ [6], spinels AB_2O_4 [7], and C15 Lave phases AB_2 [8]. Among them, Cr-based spinels ACr_2O_4 ($A = \text{Zn, Cd}$) realize the most frustrating lattice with the dominant antiferromagnetic nearest neighbor interactions due to the direct overlap of the t_{2g} orbitals of the neighboring Cr^{3+} ($3d^3$) ions [9,10]. Consequently, ACr_2O_4 remains paramagnetic to temperatures far below the characteristic strength of the interactions between the spins, the Curie-Weiss temperature $|\Theta_{\text{CW}}| = 390$ K and 88 K for $A = \text{Zn}$ [3] and Cd [11–13], respectively. Upon further cooling, however, the system undergoes a first-order spin-Peierls-like phase transition [7,14] from a cubic paramagnet to a tetragonal Néel state at $T_N = 12.5$ K and 7.8 K for $A = \text{Zn}$ [7] and Cd [12,13], respectively.

Recently, ZnCr_2O_4 has been studied extensively using neutron scattering techniques [7,15]. Its tetragonal distortion involves a contraction along the c axis ($c < a$). Its

Néel state has a rather complex commensurate spin structure. The spin structure has four different characteristic wave vectors, \mathbf{Q}_M , $(\frac{1}{2}, \frac{1}{2}, 0)$, $(1, 0, \frac{1}{2})$, $(\frac{1}{2}, \frac{1}{2}, \frac{1}{2})$, and $(0, 0, 1)$ [16]. Furthermore, the relative ratios of the neutron scattering intensities of these wave vectors vary depending on the subtle chemical conditions during sample preparation [16]. This suggests that even in the tetragonal phase, ZnCr_2O_4 is critically located close to several spin structures, that makes it difficult to understand the true nature of its ground state. The CdCr_2O_4 compound in this class has not received much attention partly because it was commonly believed that the same physics hold true as in ZnCr_2O_4 [12], which we found is not the case. As the pyrochlore lattice possesses many ground states and multiple ways for lifting the ground state degeneracy, CdCr_2O_4 provides a venue for understanding phase transitions in this seemingly complex class of materials.

In this Letter, we report the results from elastic and inelastic neutron scattering measurements on $^{114}\text{CdCr}_2\text{O}_4$ (space group $Fd\bar{3}m$, $a = 8.588\,82(5)$ Å for $T = 10$ K). Surprisingly, we find that it undergoes a phase transition that is qualitatively different in nature from the one observed in ZnCr_2O_4 . CdCr_2O_4 elongates along the c axis ($c > a$) and undergoes an incommensurate (IC) Néel order. The high \mathbf{Q} resolution data indicate that the incommensurate magnetic structure has a single characteristic wave vector of $\mathbf{Q}_M = (0, \delta, 1)$ with $\delta \sim 0.09$ perpendicular to the unique c axis. We present two possible high symmetry spin structures that are consistent with the particular \mathbf{Q}_M . The interplay between the lattice distortion and the IC spin structure is discussed along with dispersion of the spin wave excitation.

Preliminary measurements were initially performed on the TAS2 thermal triple-axis spectrometer of Japan Atomic

Energy Research Institute (JAERI), while more detailed studies ensued on the SPINS cold neutron triple-axis spectrometer of NIST Center for Neutron Research. A single crystal weighing ~ 100 mg was used for the elastic measurements, while three of these crystals were comounted within 1° mosaic for the inelastic measurements. The crystals were mounted in the $(hk0)$ scattering plane, that allowed the investigations of three equivalent $(hk0)$, $(0kl)$, and $(h0l)$ planes due to the crystallographic domains.

Figure 1 shows the \mathbf{Q} dependence of the spin fluctuations in the spin liquid phase of CdCr_2O_4 measured above T_N . The ring-shaped intensity around $(2,2,0)$ is essentially identical to the one observed in ZnCr_2O_4 , and it is due to the collective low energy excitation of antiferromagnetic hexagonal spin clusters in the pyrochlore lattice [15]. This suggests that the cubic phase of CdCr_2O_4 can be well represented by the Hamiltonian \mathcal{H}_1 as in ZnCr_2O_4 . J is estimated from the Curie-Weiss temperature $|\Theta_{\text{CW}}| = 88.97$ K [see Fig. 2(a)], to be $J = -1.02$ meV. Although CdCr_2O_4 appears to have the same fundamental spin degrees of freedom in the cubic phase as in ZnCr_2O_4 , it exhibits strikingly different behaviors in the tetragonal phase below $T_N = 7.8$ K. It undergoes an elongation along the c axis [Figs. 2(b) and 2(d)] and the magnetic long range order has an incommensurate characteristic wave vector [see Fig. 2(c)].

The positions of the magnetic Bragg reflections found in the scattering plane are shown in Fig. 3(a). The possible characteristic incommensurate wave vectors are $\mathbf{Q}_M = (0, \delta, 1)$ or $(0, 1, \delta)$ or $(1, \delta, 0)$ with $\delta = 0.0894(3)$. (h and k are interchangeable.) However, since $c > a$, the three possible \mathbf{Q}_M 's would produce the magnetic Bragg reflections at slightly different positions in the scattering plane. We performed elastic scans with a high \mathbf{Q} resolution over a set of three IC positions to distinguish between the differ-

ent scenarios. Figure 3(b) shows the results. The solid up arrows, middle dotted down arrow, and outer dashed down arrows correspond to the expected peak positions for $\mathbf{Q}_M = (0, \delta, 1)$, $(1, \delta, 0)$, and $(0, 1, \delta)$, respectively. All three of the experimental peak positions are consistent with $\mathbf{Q}_M = (0, \delta, 1)$, which indicates that the incommensurability occurs either along the a or the b axis, perpendicular to the elongated c axis. Furthermore, we have performed polarized neutron diffraction at TAS1 of JAERI (the details and results of the experiment will be reported elsewhere [17]), and found that the spins are lying on the plane that is perpendicular to the incommensurability direction. For convenience, we chose $\mathbf{Q}_M = (0, \delta, 1)$ with the spins lying in the ac plane. The resulting break-outs of the magnetic Bragg reflections into three crystallographic and two magnetic domains are shown as different symbols in Fig. 3(a).

Following group theory arguments [18], the magnetic lattice with the characteristic wave vector of \mathbf{Q}_M consists of four independent sublattices as represented by spheres with different colors in Figs. 3(c) and 3(d). Each sublattice connects every third nearest neighboring Cr^{3+} ions that are separated by the symmetrically equivalent distance of $(\frac{1}{2}, \frac{1}{2}, 0)$. These are the second nearest neighbors along the chains represented by lines in Figs. 3(c) and 3(d). Within the sublattice, spins are aligned according to $\mathbf{S}_j = \mathbf{S}_o e^{2\pi i \mathbf{Q}_M \cdot (\mathbf{r}_j - \mathbf{r}_o)}$ and therefore the neighbor spins rotate by 2α , π , and $2\alpha + \pi$ in the ab , ac , and bc plane, respectively, where $2\alpha = \delta\pi = 16.2^\circ$. In order to construct the relative orientation between the different sublattices, the magnetic interactions in the tetragonal phase of CdCr_2O_4 are considered. Analysis of a series of chromium oxides

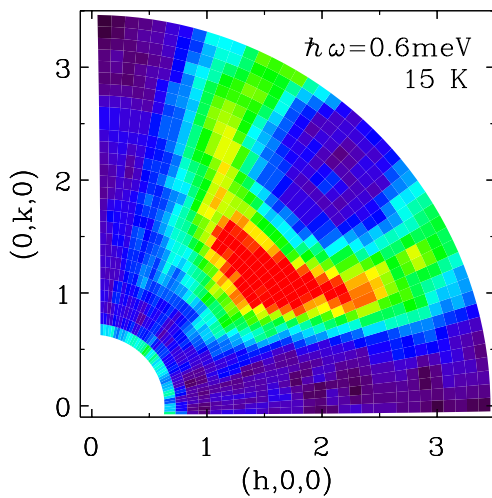


FIG. 1 (color online). Color image of inelastic neutron scattering intensities from single crystals of CdCr_2O_4 at $T = 15$ K $> T_N$ with $\hbar\omega = 0.6$ meV. The data were taken at SPINS using $11 \times 2.1 \times 15$ cm PG(002) analyzer blades with $E_f = 5$ meV.

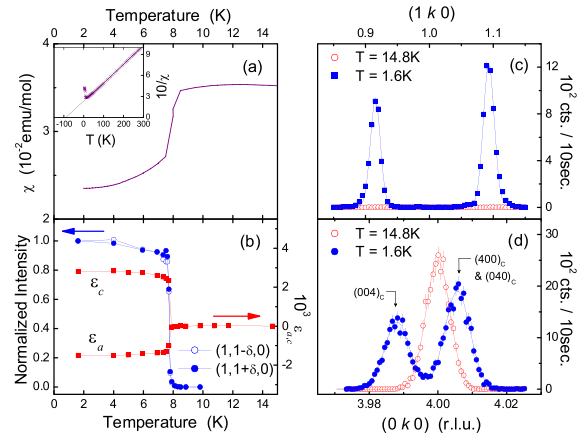


FIG. 2 (color online). (a) Bulk susceptibility, χ , as a function of T . The transition is of first-order and has a small but finite hysteresis over 0.1 degrees. The inset shows a linear fit to $1/\chi$. (b) T dependence of the normalized integrated neutron scattering intensity at the magnetic peaks and that of the lattice strains, $\epsilon_{a,c} = \frac{\Delta(a,c)}{(a,c)}$. The data were obtained from fitting the data in (c) and (d) to Gaussian peaks. (c), (d) Elastic neutron scattering data (c) through magnetic $(1, \delta, 0)$ IC points and (d) through a nuclear (400) Bragg reflection below and above T_N .

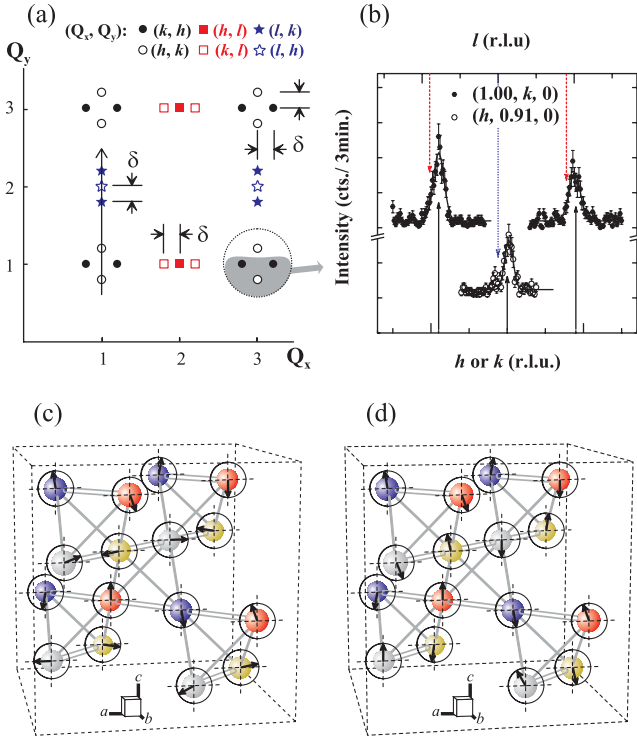


FIG. 3 (color online). (a) The observed pattern of the magnetic reflections on the scattering plane. The quadruplets consist of two doublets at $\mathbf{Q}_N \pm (0, \delta, 1)$ and $\mathbf{Q}_N \pm (\delta, 0, 1)$, respectively. The central peaks of the triplets are tails of the doublets that are present above and below the scattering plane. The symbols distinguish the crystallographic domains. (b) Elastic \mathbf{Q} scans centered at the three peaks under a gray shadow in (a). (c), (d) two possible spin structures deduced from $\mathbf{Q}_M = (0, \delta, 1)$. Spins are rotating on the ac plane. The double and single lines represent the nearest neighbor bonds in the basal ab plane with J_{ab} and out of plane with J_c , respectively. In (c) the NN spin orientations along J_c are close to perpendicular while in (d) they are close to collinear.

indicates that $dJ/dr \approx 40$ meV/Å [19]. This implies that the tetragonal distortion ($c > a = b$) yields stronger anti-ferromagnetic (AFM) interactions in the basal plane with $J_{ab} = -1.19$ meV [double lines in Figs. 3(c) and 3(d)] and weaker AFM interactions among all other spin pairs with $J_c = -0.95$ meV (single lines). For each chain in the basal plane, the nearest neighboring spins that belong to two different sublattices would favor a phase difference of $\pi \pm \alpha$ to minimize the exchange energy due to the strong AFM J_{ab} . The out-of-plane J_c is frustrating that allows stacking of the $\langle 110 \rangle$ chains along the c axis. Figs. 3(c) and 3(d) show two highly symmetric spin structures that have the same mean-field exchange energy; in one, the chains are stacked almost orthogonally along the c axis [Fig. 3(c)] and the other, the chains are stacked almost collinearly [Fig. 3(d)].

To understand the elementary excitation of the IC Néel state, constant- $\hbar\omega$ and constant- \mathbf{Q} scans were performed (Fig. 4). The constant- \mathbf{Q} scan at an IC zone center [Fig. 4(d)] shows that there is a gap, Δ , of 0.65 meV along

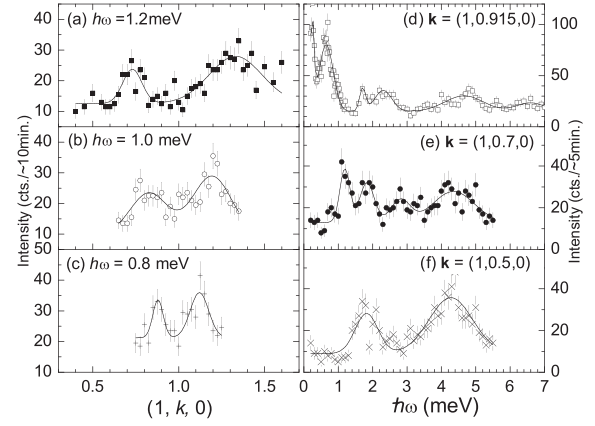


FIG. 4. Constant- $\hbar\omega$ [(a), (b), (c)] and constant- \mathbf{Q} [(d), (e), (f)] scans of the spin wave excitation in CdCr_2O_4 . The solid lines are to guide the eyes.

with at least two additional excitation peaks around 2.3 and 4.7 meV. At \mathbf{Q} values away from the zone center, the lowest energy peak shifts considerably in energy while the two higher energy peaks shift only slightly [Figs. 4(e) and 4(f)]. Figures 4(a)–4(c) show the dispersiveness at low energies. Additional scans were performed to map out the dispersion relation of the magnetic fluctuations along the $(1, k, 0)$ direction [the arrow from $\mathbf{Q}_y = 0.5$ to 2.5 in Fig. 3(a)], summarized in Fig. 5(e).

What kind of spin Hamiltonian would select the observed IC Néel state as the ground state of CdCr_2O_4 in the tetragonal phase? The exchange anisotropy of the nearest neighboring (NN) couplings, $J_c \neq J_{ab}$, alone would favor a commensurate spin structure rather than the IC one, which means that additional perturbations to \mathcal{H}_1 are present. However, $\Delta \approx 0.6$ meV is small compared to the entire energy band width of the dispersion, ~ 5 meV, which suggests that the additional perturbations must be small. Let us first discuss the effect of the exchange anisotropy of the NN couplings, $J_c \neq J_{ab}$, on the dispersion of the two model spin structures shown in Figs. 3(c) and 3(d). In the ideal isotropic case, $J_c = J_{ab}$, there is a fourfold (sixfold) degenerate flat zero-energy mode and another fourfold (twofold) degenerate dispersive mode that extends to higher energies in the orthogonal (collinear) model [Fig. 5(a)]. As the anisotropy is introduced, the zero-energy mode becomes dispersive. In the collinear structure, the sixfold zero-energy mode splits into twofold and fourfold weakly dispersive modes, whereas it remains fourfold degenerate for the orthogonal structure [20]. The dispersions are not affected by the exchange anisotropy at high energies as much as they are at low energies. Indeed, other anisotropy terms such as the single ion anisotropy and the Dzyaloshinsky-Moriya interactions also modify the dispersion at low energies considerably but not at high energies. Figure 5(d) shows the dispersion relations obtained using the experimentally determined $J_{ab} = -1.19$ meV and $J_c = -0.95$ meV. This shows

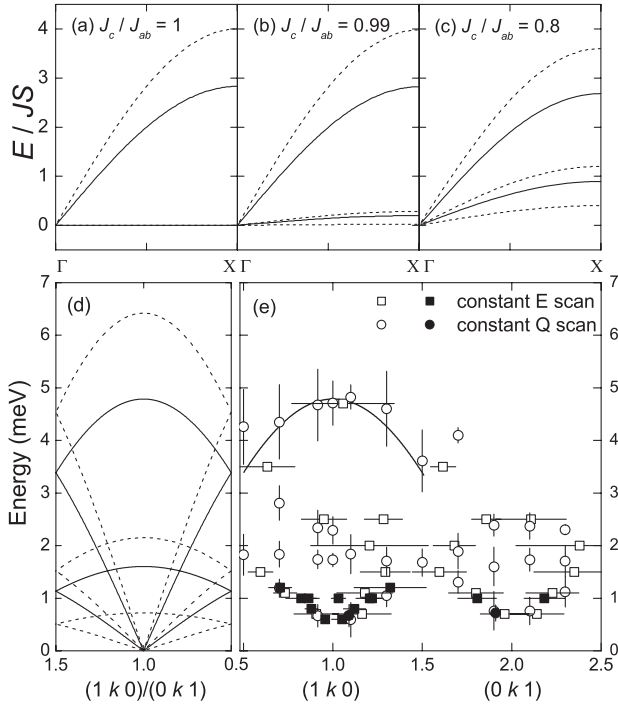


FIG. 5. (a), (b), (c), (d) The spin wave calculations with the orthogonal (solid lines) and the collinear (dashed lines) commensurate models with different ratios of J_c/J_{ab} . In (a), (b), and (c) the energy is in unit of $J_{ab}S$ while in (d) the energy is calculated in meV with $J_{ab} = -1.19$ meV and $J_c = -0.95$ meV. Since the overlap between the $(1, k, 0)$ and $(0, k, 1)$ domains is considered, the $k = 1$ point corresponds to the AFM zone center in the former case while it corresponds to the zone boundary for the latter. (e) The dispersion relations determined from constant- \mathbf{Q} and constant- $\hbar\omega$ scans. The line is a guide for the eyes. The data were taken along the direction in the \mathbf{Q} space shown as an arrow in Fig. 3(a). The open and closed symbols are the data obtained with focusing and flat analyzers, respectively.

that the orthogonal spin structure fits the dispersion at high energies better than the collinear one. This means that the Néel state of CdCr_2O_4 is likely to be the incommensurate spin structure with the orthogonal stacking shown in Fig. 3(c). The actual incommensurability seems to be caused by other perturbative terms, such as further nearest interactions and/or Dzyaloshinsky-Moriya interactions [21]. We also considered the exchange interactions between third nearest neighbor interactions, and extensively examined the phase space as a function of J . We found a region where an incommensurate spin structure can be selected as a ground state but the incommensurability was along the $\langle 110 \rangle$ direction, as recently observed in LiCuVO_4 [22], rather than the observed $\langle 010 \rangle$ direction. This suggests that the tetragonal distortion involves distortions of the oxygen octahedra that lowers the crystal symmetry.

In summary, we identified a spin-lattice coupling mechanism that lifts the magnetic frustration in CdCr_2O_4 and that is distinctly different from the one observed in ZnCr_2O_4 . The tetragonal distortion involves an elongation along the c axis and the Néel state has a helical spin structure with the single characteristic wave vector of $\mathbf{Q}_M = (0, \delta, 1)$. Our identification of the spin structure and dynamics of the low temperature phase of CdCr_2O_4 should provide a unique test to theoretical attempts to explain the spin-Peierls-like phase transitions in the Heisenberg pyrochlore antiferromagnets.

We thank C.L. Henley, Y. Motome, A. Zheludev, and D. Louca for valuable discussions. This work was partially supported by the NSF through DMR-9986442 and by the U.S. DOC through NIST-70NANB5H1152.

-
- [1] H.A. Jahn and E. Teller, Proc. R. Soc. A **161**, 200 (1937).
 - [2] Y. Tokura and N. Nagaosa, Science **288**, 462 (2000).
 - [3] A.P. Ramirez, in *Handbook of Magnetic Materials*, edited by K.H.J. Buschow (Elsevier, Amsterdam, 2001), Vol. 13, 423–520.
 - [4] R. Moessner and J. Chalker, Phys. Rev. Lett. **80**, 2929 (1998); Phys. Rev. B **58**, 12 049 (1998).
 - [5] B. Canals and C. Lacroix, Phys. Rev. Lett. **80**, 2933 (1998); Phys. Rev. B **61**, 1149 (2000).
 - [6] S.T. Bramwell and M.J.P. Gingras, Science **294**, 1495 (2001).
 - [7] S.-H. Lee *et al.*, Phys. Rev. Lett. **84**, 3718 (2000).
 - [8] R. Ballou *et al.*, Phys. Rev. Lett. **76**, 2125 (1996).
 - [9] J.B. Goodenough, Phys. Rev. **117**, 1442 (1960).
 - [10] E.J. Samuelsen *et al.*, Physica (Amsterdam) **48**, 13 (1970).
 - [11] N. Menyuk *et al.*, J. Appl. Phys. **37**, 1387 (1966).
 - [12] M.T. Rovers *et al.*, Phys. Rev. B **66**, 174434 (2002).
 - [13] H. Ueda *et al.*, Phys. Rev. Lett. **94**, 047202 (2005).
 - [14] Y. Yamashita and K. Ueda, Phys. Rev. Lett. **85**, 4960 (2000); O. Tchernyshyov *et al.*, *ibid.* **88**, 067203 (2002).
 - [15] S.-H. Lee *et al.*, Nature (London) **418**, 856 (2002).
 - [16] S.-H. Lee *et al.*, (unpublished).
 - [17] K. Kakurai *et al.*, (unpublished).
 - [18] Yu.A. Izyumov, V.E. Naish, and R.P. Ozerov, *Neutron Diffraction of Magnetic Materials* (Plenum, New York, 1991).
 - [19] K. Motida and S. Miahara, J. Phys. Soc. Jpn. **28**, 1188 (1970).
 - [20] Note that the two spin structures with $\delta = 0$ produce exactly the same spectrum along the (110) chain directions.
 - [21] C.L. Henley (private communication).
 - [22] B.J. Gibson *et al.*, Physica (Amsterdam) **350B**, E253 (2004); M. Enderle *et al.*, Europhys. Lett. **70**(2), 237 (2005); The crystal symmetry of $Imma$ was used and the $\mathbf{Q}_M = (0, \delta, 0)$ corresponds to $\frac{1}{2}(\bar{\delta}, \delta, 0)$ in the $Fd\bar{3}m$ notation.